New Journal of Physics

PAPER

CrossMark

Initialization of a spin qubit in a site-controlled nanowire quantum dot

Konstantinos G Lagoudakis[1,7], Peter L McMahon[1,7], Kevin A Fischer[1], Shruti Puri[2], Kai Müller[1], Dan Dalacu[3], Philip J Poole[3], Michael E Reimer[4], Val Zwiller[5], Yoshihisa Yamamoto[1,6] and Jelena Vučković[1]

1 E.L. Ginzton Laboratory, Stanford University, Stanford, CA 94305, USA
2 Département de Physique, Université de Sherbrooke, Sherbrooke, J1K 2R1 Québec, Canada
3 National Research Council of Canada, Ottawa, K1A 0R6, Canada
4 Institute for Quantum Computing and Department of Electrical and Computer Engineering, University of Waterloo, Waterloo, Ontario, N2L 3G1 Canada
5 Quantum Nano Photonics, KTH Royal Institute of Technology, SE-100 44 Stockholm, Sweden
6 National Institute of Informatics, Hitotsubashi 2-1-2, Chiyoda-ku, Tokyo 101-8403, Japan
7 These authors contributed equally to this work.

E-mail: lagous@stanford.edu and pmcmahon@stanford.edu

Abstract

A fault-tolerant quantum repeater or quantum computer using solid-state spin-based quantum bits will likely require a physical implementation with many spins arranged in a grid. Self-assembled quantum dots (QDs) have been established as attractive candidates for building spin-based quantum information processing devices, but such QDs are randomly positioned, which makes them unsuitable for constructing large-scale processors. Recent efforts have shown that QDs embedded in nanowires can be deterministically positioned in regular arrays, can store single charges, and have excellent optical properties, but so far there have been no demonstrations of spin qubit operations using nanowire QDs. Here we demonstrate optical pumping of individual spins trapped in site-controlled nanowire QDs, resulting in high-fidelity spin-qubit initialization. This represents the next step towards establishing spins in nanowire QDs as quantum memories suitable for use in a large-scale, fault-tolerant quantum computer or repeater based on all-optical control of the spin qubits.

Abbreviations

QD	quantum dot
InP	Indium Phosphide
InAsP	Indium Arsenide Phosphide
SCQD	site-controlled quantum dot
CW	continuous wave.

Introduction

The development of site-controlled quantum dots (QDs), and demonstration of their suitability for hosting spin-based qubits, is a key objective in the roadmap towards a scalable quantum information processing system implemented with QDs [1–3]. There has been considerable recent effort in exploring different techniques for fabricating site-controlled QDs, including lithographic patterning of growth substrates [4, 5], stress-induced

positioning within micropillars [6], and the growth of QDs within seeded nanowires [7]. QDs within nanowires have been shown to have both high photon-extraction efficiencies [8, 9], and good single-photon source characteristics [7–9]. Furthermore, magneto-photoluminescence spectroscopy studies [10, 11] of InAsP QDs in InP nanowires have shown that QDs in nanowires may be a promising platform for hosting spin qubits, but to our knowledge, thus far there have been no demonstrations of the fundamental spin manipulation operations [12–20] on spins trapped in nanowire-hosted QDs, nor in any other site-controlled QD devices. Nanowire QDs are a substantially different platform—with respect to both material and structural characteristics—than self-assembled QDs in a bulk host (the system with which the majority of spin qubit studies using optically active QDs have been performed to date). Nanowire QDs have high brightness due to the waveguiding effect of the needle-like structure in which each QD is embedded. Brightness is an advantage that nanowire QDs share with QDs embedded in micropillars, but they currently offer the additional advantage of being deterministically positionable without compromising optical quality. Here we demonstrate all-optical initialization of spin qubits embedded in several deterministically positioned InP nanowire QDs, which is a first step towards realizing more complex spin experiments with nanowire QDs, including coherent spin control [3] and spin-photon entanglement generation [2].

Methods

We studied a sample with InAsP QDs embedded in InP nanowires that was grown using vapor–liquid–solid epitaxy on a (111)B InP substrate; the growth details can be found in [7]. The substrate was covered with a SiO_2 mask containing a grid of apertures, which were produced using e-beam nanopatterning. The growth of each nanowire was seeded by placing a gold nanoparticle in the center of each aperture [7, 22, 23] and consisted of a two-step process that involves growth of a core nanowire containing the InAsP QD followed by growth of a shell, which results in the needle-like shape of the nanowires.

Photoluminescence spectra were measured using a custom double-grating spectrometer setup with ~10 μeV resolution, which is necessary in order to spectrally select just a single emission line from the QD, and measure its signal on a single-photon counter, while rejecting light from a CW laser that is used for the spin initialization and has its center frequency near the QD emission line that is being collected.

For all the experiments that required application of a magnetic field, we used the Voigt geometry, since this is the configuration that is used for spin control with optical pulses [15, 16, 18], and for generation of spin-photon entanglement [24–27].
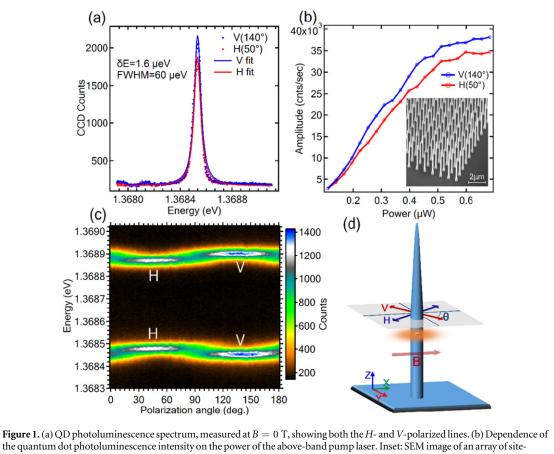
Results

In this article we present results from a typical quantum-dot-nanowire device in our sample; the QD exhibited emission under CW above-band (780 nm) excitation that was both bright and spectrally narrow. Figure 1(a) shows the polarization-resolved spectra from the QD. At saturation the QD exhibited a linewidth of ~60 μeV full-width-at-half-maximum, and an energy difference of $\delta E = 1.6$ μeV between the two orthogonal linear polarization components (measured between the fitted peak centers; see figure 1(a). The emission intensity of both H- and V-polarized lines have a linear dependence on the above-band laser power, until saturation is reached at approximately 550 nW (figure 1(b)). The linear power dependence is consistent with these lines corresponding to single exciton emission, as opposed to biexciton emission (which would exhibit a quadratic power dependence). To determine that the QD was charged, we used magneto-photoluminescence spectroscopy in the Voigt configuration (magnetic field perpendicular to the nanowire growth direction): figure 1(c) shows the photoluminescence signal from the QD as a function of its emission energy and polarization. The photoluminescence spectra clearly show a four-fold splitting, which is consistent with emission from a charged dot [28]. We note that in this figure and the remainder of the paper, we define H as the linear polarization that is $\theta = 50°$ relative to the magnetic field and V as the linear polarization that is at $\theta = 140°$ relative to the magnetic field, as shown in the illustration in figure 1(d).

We obtained further evidence that the QD was charged by recording photoluminescence spectra as a function of the applied magnetic field strength. Figure 2(a) shows the photoluminescence spectra of the QD for varying magnetic fields in the range from 0 to 5 T for both the H and V polarizations; the splitting of the emission into four lines is clearly evident. This is expected for a charged dot, for which there are two contributions to the transition energies that depend on the magnetic field: a linear dependence due to the Zeeman effect [28] (figure 2(b)), and a quadratic dependence resulting from the diamagnetic shift [29, 30], (figure 2(c)).

The four-fold splitting of the spectral lines, their linear dependence on the B-field (after the diamagnetic shift has been subtracted), their polarization properties, and their approximately equal brightness, indicate that the
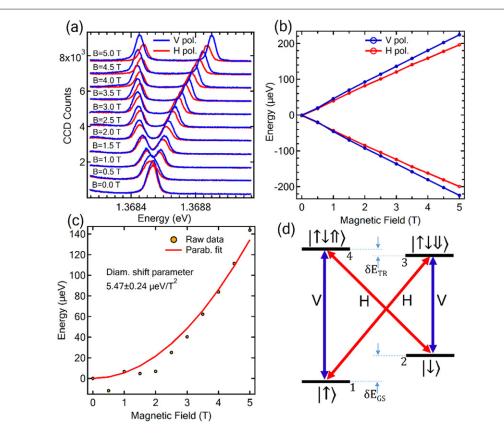
Figure 1. (a) QD photoluminescence spectrum, measured at $B = 0$ T, showing both the *H*- and *V*-polarized lines. (b) Dependence of the quantum dot photoluminescence intensity on the power of the above-band pump laser. Inset: SEM image of an array of site-controlled InP nanowires. (c) Polarization-resolved photoluminescence spectra from the quantum dot in a magnetic field of $B = 5$ T, showing four distinct spectral lines and their respective polarizations. (d) Main polarization orientations with respect to the orientation of the applied magnetic field. For this particular quantum dot, *H* is defined by $\theta_H = 50°$ and *V* by $\theta_V = 140°$.

QD has both the level structure and the selection rules of a charged QD. Figure 2(d) shows the relevant energy-level diagram for a charged QD in a Voigt-configuration magnetic field [28], and the polarization selection rules for the optical transitions.

Figure 3 illustrates our spin-pumping experiments, and shows the main results. We performed a set of four different experiments, to demonstrate that we can perform spin pumping into either the $|\uparrow\rangle$ state or the $|\downarrow\rangle$ state, in each case using one of two (per spin state) available optical transitions. The inset of figure 3(a) illustrates the QD optical transitions we used for pumping and detection in one of the four experiments, and we use it here as an example case to describe the experiment in detail. The principle of the experiment is as follows [31, 32]. A fixed-wavelength above-band laser is used to randomize the state of the spin; it does this by incoherently exciting states at far higher energies than the QD trion levels, and through a series of decay processes, some of which are non-spin-preserving, the QD trion levels are randomly populated, and these levels in turn decay and randomly populate the QD ground-state spin levels. The action of the spin-randomization laser is depicted as violet upward wavy arrows. A tunable laser is used to resonantly excite one of the trion states via a vertical transition $(|\uparrow\rangle - |\uparrow \downarrow \Uparrow\rangle)$. If the system is initially in the state $|\uparrow\rangle$, then this laser will cause the trion state $|\uparrow \downarrow \Uparrow\rangle$ to be populated. This trion state will then decay to either the $|\downarrow\rangle$ or $|\uparrow\rangle$ state with equal probability (gray downward wavy arrows in the inset of figure 3(a)). If the decay is to the state $|\uparrow\rangle$, then the tunable laser will re-excite the trion state. If, on the other hand, the decay is to the $|\downarrow\rangle$ state, then the tunable laser will no longer be resonant with any transition and the system will be initialized in the $|\downarrow\rangle$ state, until the spin is randomized again. The emission from the $|\uparrow \downarrow \Uparrow\rangle - |\downarrow\rangle$ transition is spectrally filtered and sent to a single-photon counter, providing a measurement of the spin state [3].

Figure 3(a) shows the collected photon counts as a function of the wavelength of the spin-pumping laser, as it was tuned over the $|\uparrow\rangle - |\uparrow \downarrow \Uparrow\rangle$ transition. Two traces are shown: one when only the spin-pumping laser was on (in blue), and one when both the randomization laser and the spin-pumping laser were on (in red). When both lasers were on, the data (red points) show a clear resonance, corresponding to spin-pumping-laser photons being absorbed by the $|\uparrow\rangle - |\uparrow \downarrow \Uparrow\rangle$ transition, and being emitted by the $|\uparrow \downarrow \Uparrow\rangle - |\downarrow\rangle$ transition. The reason that photons can be absorbed by the $|\uparrow\rangle - |\uparrow \downarrow \Uparrow\rangle$ transition is that the $|\uparrow\rangle$ state is continually being populated as a result of the randomization laser being on. However, when the randomization laser is turned off, the data
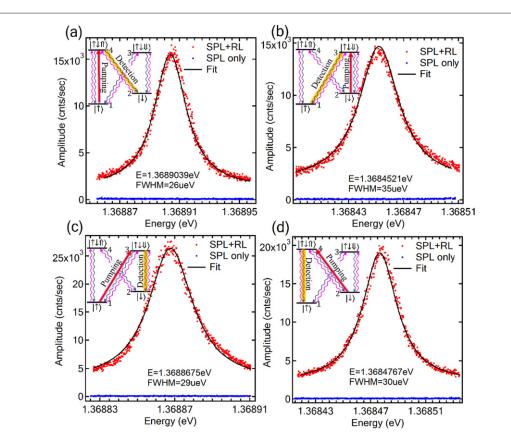
Figure 2. Voigt configuration magneto-photoluminescence spectra of the QD in a nanowire. (a) Raw spectra of photoluminescence at various magnetic fields *B*. (b) Energy shift of the optical transitions versus magnetic field, after subtraction of the diamagnetic shift. The linear dependence arises due to the Zeeman splitting of both the ground states and trion states. (c) The quadratic energy shift of the spectral lines due to the diamagnetic shift. (d) Energy level diagram of spin and trion states in a charged quantum dot, in a Voigt-configuration magnetic field (*B* perpendicular to the nanowire growth direction). All four optical transitions are allowed, and the polarization selection rules are indicated. δE_{gs} is the ground state Zeeman splitting and δE_{tr} the trion state Zeeman splitting.

(blue points) shows no resonance as the spin-pumping laser passed over the $|\uparrow\rangle - |\uparrow\downarrow\Uparrow\rangle$ transition. This serves as strong evidence that the QD spin has in this case been optically initialized in the $|\downarrow\rangle$ state. (The intuitive reasoning behind this claim is that if the spin is initialized in the $|\downarrow\rangle$ state, then no further photons from the spin-pumping laser can be absorbed, so in the absence of the randomization laser, there will be no excitation of the QD, and hence no photons emitted. In contrast, if the spin was being imperfectly initialized, or the spin relaxation time was very short, then one should expect to observe photons being emitted when the spin-pumping laser is on resonance with the $|\uparrow\rangle - |\uparrow\downarrow\Uparrow\rangle$ transition. Our data are therefore consistent with our having successfully initialized the spin.)
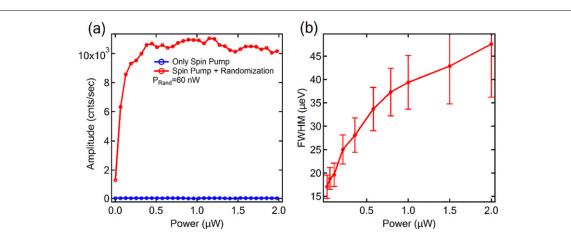
In an analogous manner, figure 3(b) shows how the QD spin can be optically pumped into the $|\uparrow\rangle$ state via the other vertical optical transition ($|\downarrow\rangle - |\uparrow\downarrow\Downarrow\rangle$), and figures 3(c) and (d) show how the QD spin can be optically pumped using the two available diagonal optical transitions.

To demonstrate the robustness and repeatability of this spin qubit initialization technique in nanowire QDs, we performed the same type of optical pumping experiments on several nanowire QDs on the same sample, which yielded essentially identical results to those shown in figure 3 (see supplementary data).

To further characterize the spin pumping process, we also studied the spin-pumping signal as a function of the applied spin-pumping-laser power. Figure 4 shows the dependence of the peak spin-pumping signal on the spin-pumping-laser power in the experiment in figure 3(a) (where the spin is pumped into the $|\downarrow\rangle$ state using the $|\uparrow\rangle - |\uparrow\downarrow\Uparrow\rangle$ transition). In particular, the red data points in figure 4(a) show that the peak of the spin-pumping signal initially increases rapidly with applied laser power, and saturates once the spin-pumping-laser power reaches approximately 350 nW. The blue data points are from the same experiment, except the randomization laser had been turned off. We note that even with a power well above the value that is sufficient to saturate the $|\uparrow\rangle - |\uparrow\downarrow\Uparrow\rangle$ transition (and hence cause maximal spin pumping), when the randomization laser is off, there is no increase in the counts as a function of power, which is consistent with high-fidelity optical pumping and excellent spectral-filtering-based rejection of the scattered spin-pumping-laser light. We also studied the effect of the applied laser power on the width of the transition resonance. Figure 4(b) shows the full-width-at-half-maximum linewidth of the resonance when both the randomization laser and the spin-pumping laser were on,

Figure 3. Spin-pumping and measurement experiment, for four different spin-pumping laser configurations. (a)–(d) Detected photons as a function of the spin-pumping-laser energy, for the specific experimental protocols illustrated in the respective insets. Red data points show the collected photon counts when both lasers were on, whereas the blue data points show the photon counts when only the spin-pumping laser was on. For all four spin pumping schemes the powers used were $P_{\text{spin-pump}} = 500$ nW (spin-pumping laser) and $P_{\text{rand}} = 60$ nW (above-band spin randomization laser). The insets are showing the relevant levels of the quantum dot, the applied laser fields, and photon collection. The net effect of the spin randomization laser (above-band excitation that decays randomly into the two trion states; see main text for details) is shown as upward violet wavy arrows. Spontaneous decay is depicted as downward gray wavy arrows. A tunable CW laser ('Pumping'), is scanned across one of the optical resonances. Photons emitted by the yellow shaded transition ('Detection') are collected, and measured by a single-photon counter.

Figure 4. Spin-pumping peak amplitude and width as a function of the power of the spin-pumping laser, in the experiment described in figure 3. The randomization laser power was kept constant at $P_{\text{rand}} = 60$ nW. (a) Red: photon counts at the peak of the spin-pumping resonance (when both lasers were on), as a function of the spin-pumping laser power. Blue: photon counts measured when the randomization laser was off. (b) The full-width-at-half-maximum linewidth of the resonance shown in figure 3(a), as a function of the spin-pumping laser power.

as a function of the power of the spin-pumping laser. At lower powers ($P_{\text{spin-pump}} < 0.15~\mu$W), we observed a linewidth of less than 20 μeV, with substantial broadening as the power was increased to be above the saturation limit of the transition. The power-dependence measurements in figures 1(b) (above-band excitation photoluminescence power dependence) and 4(a) (spin-pumping laser power dependence) provide valuable

information for quantitatively assessing the efficacy of the spin pumping process, since the saturation values can be used to infer the relative rates of spin pumping and spin randomization.

We have used a rate-equation model (described in detail in the supplementary data) of the spin pumping experiment to analyze our experimental results; it shows that our data is consistent with optical spin pumping causing spin qubit initialization with a fidelity of 99% in less than 10 ns. This is similar to the reported performance of spin pumping in self-assembled InAs QDs [13, 16, 18]. We used our model to infer a lower bound on the spin lifetime of $T_1 > 3~\mu s$. These values suggest promise for the use of charges in nanowire QDs as spin qubits.

Conclusion

As is the case with micropillar QDs, the structural characteristics of nanowire QDs render them incompatible with most scalable two-qubit gate proposals for spin qubits, due to the lack of a direct way for the trapped electrons (or holes) to interact. Spin qubits in nanowire QDs (and micropillar QDs) are thus perhaps better suited to quantum computing or repeater architectures in which the stationary qubits are entangled indirectly, by interfering and detecting photons that are entangled with the spins [2], which is also the one of the leading approaches for scaling free-space trapped-ion qubits [21]. Our experiments make a contribution towards the intermediate-term goal of entangling two spatially separate QD spins on a single chip by showing that one of the steps of the entanglement-generation protocol—spin initialization—can be performed with QDs that are deterministically positioned and have high brightness. In this paper we have demonstrated that in the InAsP-QD/InP-nanowire system a charged QD in a Voigt magnetic field does yield two optical Λ-systems that can be manipulated, and we have demonstrated optical spin pumping using independent experiments on both transitions in both Λ-systems. Using several different nanowires, we were able to show that spin measurement as part of the optical pumping process is possible in the InAsP-QD/InP-nanowire system. These experiments were all performed on site-controlled nanowires, making this the first demonstration, to our knowledge, of optical pumping of site-controlled QD spins.

References

[1] Jones N C, Van Meter R, Fowler A G, McMahon P L, Kim J, Ladd T D and Yamamoto Y 2012 Layered architecture for quantum computing *Phys. Rev.* X **2** 031007
[2] McMahon P L and De Greve K 2015 Towards quantum repeaters with solid-state qubits: spin-photon entanglement generation using self-assembled quantum dots *Engineering the Atom-Photon Interaction* (Berlin: Springer) pp 365–402 (arXiv:1501.03535)
[3] De Greve K, Press D, McMahon P L and Yamamoto Y 2013 Ultrafast optical control of individual quantum dot spin qubits *Rep. Prog. Phys.* **76** 092501
[4] Kiravittaya S, Rastelli A and Schmidt O G 2009 Advanced quantum dot configurations *Rep. Prog. Phys.* **72** 046502
[5] Juska G, Dimastrodonato V, Mereni L O, Gocalinska A and Pelucchi E 2013 Towards quantum-dot arrays of entangled photon emitters *Nat. Photon.* **7** 527–31
[6] Strittmatter A 2012 Site-selective growth of single quantum dots *Phys. Status Solidi* a **209** 2378–2378
[7] Dalacu D, Mnaymneh K, Lapointe J, Wu X, Poole P J, Bulgarini G, Zwiller V and Reimer M E 2012 Ultraclean emission from InAsP quantum dots in defect-free wurtzite InP nanowires *Nano Lett.* **12** 5919–23
[8] Reimer M E, Bulgarini G, Akopian N, Hocevar M, Bavinck M B, Verheijen M A, Bakkers E P A M, Kouwenhoven L P and Zwiller V 2012 Bright single-photon sources in bottom-up tailored nanowires *Nat. Commun.* **3** 737
[9] Claudon J, Bleuse J, Malik N S, Bazin M, Jaffrennou P, Gregersen N, Sauvan C, Lalanne P and Gérard J-M 2010 A highly efficient single-photon source based on a quantum dot in a photonic nanowire *Nat. Photon.* **4** 174–7
[10] Witek B J, Heeres R W, Perinetti U, Bakkers E P A M, Kouwenhoven L P and Zwiller V 2011 Measurement of the *g*-factor tensor in a quantum dot and disentanglement of exciton spins *Phys. Rev.* B **84** 195305
[11] van Weert M H M, Akopian N, Perinetti U, van Kouwen M P, Algra R E, Verheijen M A, Bakkers E P A M, Kouwenhoven L P and Zwiller V 2009 Selective excitation and detection of spin states in a single nanowire quantum dot *Nano Lett.* **9** 1989–93
[12] Atatüre M, Dreiser J, Badolato A, Högele A, Karrai K and Imamoglu A 2006 Quantum-dot spin-state preparation with near-unity fidelity *Science* **312** 551–3

[13] Xu X, Wu Y, Sun B, Huang Q, Cheng J, Steel D G, Bracker A S, Gammon D, Emary C and Sham L J 2007 Fast spin state initialization in a singly charged InAs-GaAs quantum dot by optical cooling *Phys. Rev. Lett.* **99** 097401

[14] Gerardot B D, Brunner D, Dalgarno P A, Öhberg P, Seidl S, Kroner M, Karrai K, Stoltz N G, Petroff P M and Warburton R J 2008 Optical pumping of a single hole spin in a quantum dot *Nature* **451** 441–4

[15] Berezovsky J, Mikkelsen M H, Stoltz N G, Coldren L A and Awschalom D D 2008 Picosecond coherent optical manipulation of a single electron spin in a quantum dot *Science* **320** 349–52

[16] Press D, Ladd T D, Zhang B and Yamamoto Y 2008 Complete quantum control of a single quantum dot spin using ultrafast optical pulses *Nature* **456** 218–21

[17] Press D, De Greve K, McMahon P L, Ladd T D, Friess B, Schneider C, Kamp M, Höfling S, Forchel A and Yamamoto Y 2010 Ultrafast optical spin echo in a single quantum dot *Nat. Photon.* **4** 367–70

[18] De Greve K *et al* 2011 Ultrafast coherent control and suppressed nuclear feedback of a single quantum dot hole qubit *Nat. Phys.* **7** 872–8

[19] Kim D, Carter S G, Greilich A, Bracker A S and Gammon D 2011 Ultrafast optical control of entanglement between two quantum-dot spins *Nat. Phys.* **7** 223–9

[20] Lagoudakis K G, Fischer K A, Sarmiento T, Mueller K and Vučković J 2014 Hole-spin pumping and repumping in a p-type δ-doped InAs quantum dot *Phys. Rev. B* **90** 121402

[21] Monroe C and Kim J 2013 Scaling the ion trap quantum processor *Science* **339** 1164–9

[22] Borgström M T, Immink G, Ketelaars B, Algra R and Bakkers E P A M 2007 Synergetic nanowire growth *Nat. Nano* **2** 541–4

[23] Dorenbos S N *et al* 2010 Position controlled nanowires for infrared single photon emission *Appl. Phys. Lett.* **97** 171106

[24] De Greve K *et al* 2012 Quantum-dot spin-photon entanglement via frequency downconversion to telecom wavelength *Nature* **491** 421–5

[25] Gao W B, Fallahi P, Togan E, Miguel-Sanchez J and Imamoglu A 2012 Observation of entanglement between a quantum dot spin and a single photon *Nature* **491** 426–30

[26] De Greve K *et al* 2013 Complete tomography of a high-fidelity solid-state entangled spin–photon qubit pair *Nat. Commun.* **4** 2228

[27] Schaibley J R, Burgers A P, McCracken G A, Duan L-M, Berman P R, Steel D G, Bracker A S, Gammon D and Sham L J 2013 Demonstration of quantum entanglement between a single electron spin confined to an InAs quantum dot and a photon *Phys. Rev. Lett.* **110** 167401

[28] Bayer M *et al* 2002 Fine structure of neutral and charged excitons in self-assembled In(Ga)As/(Al)GaAs quantum dots *Phys. Rev. B* **65** 195315

[29] Walck S N and Reinecke T L 1998 Exciton diamagnetic shift in semiconductor nanostructures *Phys. Rev. B* **57** 9088–96

[30] Schulhauser C, Haft D, Warburton R J, Karrai K, Govorov A O, Kalameitsev A V, Chaplik A, Schoenfeld W, Garcia J M and Petroff P M 2002 Magneto-optical properties of charged excitons in quantum dots *Phys. Rev. B* **66** 193303

[31] Happer W 1972 Optical pumping *Rev. Mod. Phys.* **44** 169–249

[32] Sleiter D J, Sanaka K, Kim Y M, Lischka K, Pawlis A and Yamamoto Y 2013 Optical pumping of a single electron spin bound to a fluorine donor in a ZnSe nanostructure *Nano Lett.* **13** 116–20